Full title: Substrate traits govern the assembly of microbial community engaged in metabolic division of labor

Running title: Substrate traits govern community assembly

Miaoxiao Wang[1, 2, 3, 4], Xiaoli Chen[1, 5], Yong Nie[1#] and Xiao-Lei Wu[1, 5, 6#]

[1] College of Engineering, Peking University, Beijing 100871, China

[2] Department of Environmental Systems Science, ETH Zurich, Zurich, Switzerland

[3] Department of Environmental Microbiology, Eawag, Dübendorf, Switzerland

[4] College of Architecture and Environment, Sichuan University, Chengdu, China

[5] Institute of Ocean Research, Peking University, Beijing 100871, China

[6] Institute of Ecology, Peking University, Beijing 100871, China

[#]Corresponding author: Research Scientist, College of Engineering, Peking University.

Tel: +86 10-62759047; Fax: +86 10-62759047; E-mail: nieyong@pku.edu.cn

[#]Corresponding author: Professor, College of Engineering, Peking University.

Tel: +86 10-62759047; Fax: +86 10-62759047; E-mail: xiaolei_wu@pku.edu.cn

Abstract

Metabolic division of labor (MDOL) is widespread in nature, whereby a complex metabolic pathway is shared between different strains within a community for mutual benefit. However, little is known about how microbial populations engaged in MDOL assemble into mutually beneficial communities. We hypothesized that when degradation of an organic compound is carried out via MDOL, substrate concentration and its toxicity modulate the benefit allocation between the two microbial populations, thus governing the assembly of this community. We tested this hypothesis by combining mathematical modelling with experiments using an engineered synthetic microbial community. Numerous modelling analyses suggested that the proportion of the population executing the first metabolic step can be simply estimated by Monod-like formulas governed by substrate traits. The model and the proposed formula quantitatively predicted the assembly of our synthetic community composed of two strains degrading salicylate through MDOL. Individual-based modelling and colony pattern formation assays further indicated that our rule is also applicable to estimating community assembly in spatially structured environments. Our results demonstrate that the structure of the microbial communities can be quantitatively predicted from simple environmental factors, such as substrate concentration and its toxicity, which provides novel perspectives on understanding the assembly of natural communities, as well as insights into how to manage artificial microbial systems.

Introduction

In natural environments, microorganisms rarely live autonomously; instead, they interact with other individuals to form complex communities, in which they secrete a variety of toxins to compete with each other, or share metabolites to mutually benefit their survival. Among diverse modes of microbial interaction, metabolic division of labor (MDOL) is one of the most widespread phenomena, where distinct populations perform different but complementary steps of the same metabolic pathway[1-4]. MDOL controls numerous ecologically and environmentally important biochemical processes. For example, the nitrification pathway is often operated by the collaboration between two populations, in which the first group oxidizes ammonia to nitrite, before being converted to nitrate by another bacterial group[5]. Similarly, during the Deepwater Horizon oil spill Gulf of Mexico (2010), complete degradation of polycyclic aromatic hydrocarbons (PAHs) required the partitioning of key pathway steps into several bacterial groups[6]. Since each population only contains a subset of genetic components required for the overall pathway, MDOL is thought to be a key evolutionary strategy to reduce metabolic burden of each individual[7, 8]. In addition, bacteria have been found to use this strategy to reduce the inter-enzyme competition and the inhibitory effects of intermediates, thus improving the systematic metabolic efficiency[9]. Furthermore, MDOL vastly enhances functional differentiation of microbial communities, contributing to genetic diversity in complex ecosystem[7, 8]. Nevertheless, how microbial communities engaged in MDOL assemble in the first place remains ill-defined. Understanding the assembly rules of communities engaged in

MDOL is fundamental for better evaluating their contribution to the natural biochemical cycle.

One important aspect of microbial metabolism implemented by MDOL is the degradation of a variety of organic compounds, including PAHs [10, 11], pesticide [12-15], plastics [16], antibiotics [17], or lignocellulose [18]. Bacterial degradation of these complex substrates is usually mediated by long metabolic pathways via a number of intermediates. While these pathways often remain intact within one population, they are frequently found segregated across different members within a community, whereby the intermediates are being secreted by one species, before being degraded as substrate by another species for further processing along the same pathway. Typical examples include syringate degradation via sequential cross-feeding between *Acetobacterium woodii* and *Pelobacter acidigallici* [10], phenanthrene degradation between *Marinobacter* sp. N4 and other PAH-degrading microbes in marine environments [11], as well as atrazine degradation through MDOL within four bacterial species[14]. In most of these cases, resource allocation among different community members hold one typical feature: direct carbon sources that support bacterial growth, such as small organic acids or coenzyme A, are normally present as the final product of a pathway (Supplementary Figure 1); therefore, the population performing the last steps can preferentially acquire and privatize these nutrients (which we henceforth call *product privatization*), thus acquiring the greater benefit, while other members have to collect nutrients released from this population (Figure 1; left of the first row). We thus hypothesized that this uneven allocation of limiting resource largely determines the

87 relative fitness of strains engaged in MDOL, and thus govern the assembly of these
88 communities.
89 The findings in recent studies on MDOL communities are largely consistent with our
90 hypothesis. For instance, one earlier study developed a dual-species community for
91 biodegradation of the insecticide parathion [15]. In this consortium, an *Escherichia coli*
92 strain SD2 was responsible for hydrolyzing parathion, yielding two intermediates
93 including p-nitrophenol, while another *Pseudomonas putida* strain KT2440 was
94 responsible for metabolizing p-nitrophenol. That study found that the strain KT2440
95 that largely dominated the biofilm formed by this community. Another study
96 investigated the interactions among five bacterial species in a cellulose-degrading
97 community, which also found that the strains responsible for the last step of the
98 cellulose degradation constituted more than 60 percent of the total population [19]. In
99 addition, one study used a mathematical model to capture the dynamics of a MDOL
100 community degrading fenitrothion, in which the final product, methylhydroquinone
101 served as the common resource for the two community members [12]. That study found
102 that the strain executing the last step overwhelmingly dominated the community in most
103 of the simulations. On the basis of this finding, the study proposed that the coexistence
104 of two members requires the second member excreting sufficient amounts of
105 methylhydroquinone in order to support the growth of another member. Overall, these
106 findings suggest that our hypothesized 'Embezzler behavior' may be a common
107 phenomenon that occurs when a microbial community adopt MDOL strategy to degrade
108 organic compounds. Since 'product privatization' is a purely selfish trait, we named the

final strain at the end of a MDOL-enabled pathway the 'Embezzler', analogous to a human worker responsible for the final step of an assembly line, who pockets the final product and fails to share profits with other workers.

We also derived two corollaries based on this hypothesis. Firstly, increasing concentration of the substrate improves the flux of the pathway. Because the Embezzler only have a limited capacity of consuming the final product, more end product is released from the 'Embezzler' strain, in turn facilitating the growth of the other population (Figure 1; Right of the first row). In natural environments, the concentration of the initial substrate, such as PAHs and other hydrocarbons, is highly fluctuating over time and different sites in the marine[20], soil[21] and wastewater[22] environments. Therefore, it is crucial to understand how this variable environmental factor affect the relative fitness of strains engaged in MDOL, and thus govern the assembly of these communities. Secondly, many initial substrates that can be degraded through MDOL, such as PAHs [23, 24], are toxic to bacterial cells, inhibiting their growth. We proposed that the population performing the first step is favored when the initial substrate is toxic. Because its ability of transforming the initial substrate to the intermediates will help it possess a lower intracellular concentration of the toxic substrate (Figure 1; The second row), resulted in that the toxic substrate is generally less harmful to Detoxifier than to Embezzler. Also because of this feature, we named the population executing the first metabolic step 'Detoxifier'. In summary, in presence of the resource privatization by the 'Embezzler' population, concentration and toxicity of the substrate can be two key factors that govern the assembly of organic compound degradation community engaged

in MDOL. The goal of this study is to test this prediction.

Microorganisms often live in spatially structured environments, forming well-organized biofilms[25, 26]. In these spatially structured habitats, mass diffusion is largely limited, driving to heterogeneous distribution of the substrates and metabolites, which have large impacts on the outcomes of the metabolic exchanges between different microbial cells [27], and further govern the assembly and productivity of such communities [26, 28-30]. Particularly, since the intermediates and the product are required to be exchanged between different community members, the assembly of community engaged in MDOL should be also affected by the limited mass diffusion. For example, a recent study investigated how a well-defined community executing toluene degradation through MDOL spatially self-organized on surface, which suggested that MDOL generally favored strong intermixing between the two strains involved to facilitate their metabolic exchange [31]. Therefore, it is also important to investigate how levels of substance diffusion level in the spatially structured environment affect the assembly of MDOL communities.

Here, we set out to investigate how substrate traits drive assembly of microbial community engaged in MDOL by combining mathematical modelling and experimentation using a synthetic microbial community. We also tested whether these effects are different when the community grows in spatially well-mixed and structured environments.

Results

Testing of our prediction in well-mixed system

An ODE model for the assembly of microbial community engaged in MDOL

To test our hypothesis about Embezzler behavior, as well as the effects of substrate concentration and its toxicity, we first built a mathematical model to simulate the assembly of a community engaged in metabolic division of labor (MDOL) in a well-mixed batch culture system. The dimensionless form of this model is composed of 11 ordinary differential equations (ODEs; Eqn [3]-Eqn [13] in Methods). As summarized in Figure 2A, we considered the degradation of an organic substrate (S) into an intermediate metabolite (I) by one enzyme (E1), before being degraded to the final product (P) by a second enzyme (E2). We assumed that two strains carried out this pathway via MDOL, with the first strain only expressing E1, and the second only expressing E2. Initially, only S was supplied and the initial concentration was parameterized by s_0 (nondimensional). In addition, transport of S, I, and P across the cell membrane was assumed to occur via passive diffusion. Importantly, based on our hypothesis of 'Embezzler behavior', we assumed that, P, which was synthesized by the second strain, was the sole available resource for the growth of both strains, while neither S nor I could be directly used for growth. As a result, the second strain possessed the advantage of preferentially acquiring the resource, while the first strain only obtained those growth-limiting resource that were secreted from the second strain. Therefore, the second strain behaved as an 'Embezzler'. Moreover, biotoxicity of the substrate was imposed by adding three different toxic terms (Supplementary Table 3;[32]) to the growth function, and the toxic strength was mediated by parameter θ. Thus, for the scenarios where substrate is assumed to be toxic, the strain executing the

first step behaved as a 'Detoxifier'. Details about the model construction are described in Supplementary Information S1.

Analysis of the ODE model indicates initial substrate concentration affects the assembly of MDOL community.

To test our basic hypothesis about Embezzler behavior, as well as our corollary 1 stating that substrate concentration affects the assembly of the community, we analyzed our ODE model omitting substrate toxicity (Figure 2A). As the dimensionless model contains 11 independent parameters (Supplementary Table 4) that may affect the outcomes of community assembly, we performed a first round of numerical simulations using 885,735 parameter sets considering realistic value ranges of all the 11 parameters (Supplementary Information S1.3; Supplementary Table 4). Our analysis showed that the Embezzler population dominated the steady-state community in all these simulations (Supplementary Figure 2; no toxic scenarios, i.e., steady-state frequencies of Detoxifier are lower than 0.5), which was in agreement with our basic hypothesis of 'Embezzler behavior'. We then assessed the relative importance of the involved parameters by performing multivariate regression analyses, and found that six key parameters played vital roles in governing the assembly of MDOL community (Supplementary Table 4; Supplementary Figure 3A; $p < 0.01$ and the fitting coefficient values over 0.01). Notably, we found that s_0 was one of these key parameters (second most important according to the absolute value of the fitting coefficient). As shown in Supplementary Figure 3A and Supplementary Table 4, s_0 positively correlated with the steady-state proportion of the Detoxifier population, suggesting that a higher initial

substrate concentration favors the Detoxifier, consistent with our corollary 1.

To investigate how initial substrate concentration affects the assembly of a MDOL community, we performed second round of simulations using newly-designed 163,296 parameter sets that included more testing values of the six key parameters (Supplementary Information S1.3). We found that when all other five key parameters were kept constant, the steady-state proportion of the Detoxifier population increased with an increase of the initial substrate concentration (Figure 2B and 2C), and can be estimated by a Monod-like formula using s_0 as the function argument (Figure 2C),

$$DF = \frac{Fd_{max} \cdot s_0}{ks + s_0} \quad [1]$$

Here, DF represents the steady-state proportion of the Detoxifier population; Fd_{max} represents the maximum proportion of the Detoxifier populations when substrate is non-toxic; ks represents the half-saturation constant. Our analysis indicated that the simulation results of all tested parameter sets can be accurately fitted to Eqn. [1] (Figure 2D, values of Adjusted R^2 mostly over 0.95), although the best fitting of Fd_{max} and ks were affected by the values of other five key parameters (Figure 2E and 2F; Supplementary Information S1.3; Supplementary Table 5; Supplementary Figure 4-5). Together, these results suggest that, in the absence of substrate toxicity, the proportion of the Detoxifier population increases nonlinearly with the increase of the initial substrate concentration, and maintains a maximum value (Fd_{max}).

To investigate why substrate concentration governs the community assembly, we next analyzed the dynamics of intracellular and extracellular product concentration of the two populations.

219 We found that with the increase of initial substrate concentration, the fraction of final
220 product released by the Embezzler population (that is, the ratio of extracellular to
221 intracellular concentration) increased (Supplementary Figure 6A-H; Supplementary
222 Figure 6I, Red dots). As a consequence, the Detoxifier obtained more product from the
223 environment, resulting in a higher intracellular product concentration, which gradually
224 approached that of the Embezzler (Supplementary Figure 6A-H; Supplementary Figure
225 6I, blue dots). Therefore, consistent with our corollary 1, increasing the initial substrate
226 concentration increases the amount of the final product released by the Embezzler
227 population, thus favoring the Detoxifier. Moreover, we also found that even if the
228 substrate concentration was elevated to high levels, the intracellular product
229 concentration of the Detoxifier never exceeded that of the Embezzler, even if the
230 substrate concentration was elevated to high levels (Supplementary Figure 6A-H;
231 Supplementary Figure 6I, blue dots). As a result, Embezzler cells still maintained their
232 growth advantage from privatizing final product. This result suggests that in the absence
233 of substrate toxicity, the benefit from product privatization obtained by the Embezzler
234 strain cannot be completely eliminated by simply increasing initial substrate
235 concentrations. This observation also matched with our result that the maximum
236 proportion of the Detoxifier population (Fd_{max}) never exceeded 0.5 (Figure 2F;
237 Supplementary Figure 5). In addition, based on this mechanism, increasing the P
238 consuming capacity of Embezzler may cause less release of P to environment, thus
239 harming the Detoxifier. This corollary is supported by our observation that the value of
240 Fd_{max} was strongly negatively correlated with the consuming rate of the final product

(Cp), and ks was positively correlated with Cp (Supplementary Table 5; Supplementary Figure 4A-B; Supplementary Figure 5A-B). In summary, these results suggested that substrate concentration governs the assembly of microbial community engaged in MDOL by affecting the amount of the final product supplying from Embezzler to Detoxifier (Figure 1; the first row).

Analysis of the ODE model indicates that substrate toxicity also affects the assembly of MDOL community.

To test our corollary 2, we next employed an ODE model that included the parameter of substrate toxicity to test our corollary 2 (Figure 3A). Applying similar simulation and analysis method as used in the above section (Supplementary Information S1.3), we found that in addition to the six key parameters identified above, the toxic strength (θ) of substrate also played a significant role in governing the assembly of our MDOL community, exhibiting a significantly positive relationship with the final proportion of the Detoxifier population (Figure 3B; Supplementary Figure 2-3; Supplementary Table 4), which is in agreement with our corollary 2. We then upgraded Eqn. [1] to collectively consider the effects of substrate concentration and its toxicity (Figure 3C)

$$DF = \frac{Fd_{max} \cdot s_0}{ks + s_0} \cdot (1 + \frac{Ts_{max} \cdot \theta s_0}{kt + \theta s_0}) \quad [2]$$

In Eqn. [2], we use term $1 + \frac{Ts_{max} \cdot \theta s_0}{kt + \theta s_0}$ to describe the effect of substrate toxicity on the proportion of the Detoxifier populations, in which Ts_{max} represents the maximum fold increase of Detoxifier proportion benefiting from the substrate toxicity and ks represents the half-saturation constant of this toxic effect. This term is positively affected by the toxic strength (θ) and substrate concentration (s_0), since increasing

either toxic strength or substrate concentration harms population growth, according to our model assumptions (see Eqn. [12]-[13] in Methods and Supplementary Table 3). We next tested the applicability of Eqn. [2] on prediction of assembly of MDOL community by performing numerical simulations using 8,328,096 parameter sets (Supplementary Information 1.3). These sets included 7,776 different combinations of other five key parameters and considered three different equation forms (Supplementary Table 3) that quantified how substrate toxicity affects population growth. The results indicated that the simulation results also accurately fitted to Eqn. [2] (Figure 3D; values of Adjusted R^2 mostly over 0.90). We also assessed the main factors that affect the best fitting values of the parameters in Eqn. [2] (Supplementary Information S1.3; Supplementary Table 5; Supplementary Figure 7-10). In agreement with our results from the model omitting substrate toxicity, we found that the value of Fd_{max} still negatively correlated with the consuming rate of the final product (Cp), and ks was positively correlated with Cp (Supplementary Table 5; Supplementary Figure 8-9). These results suggest that in the when substrate toxicity was taken into account, the proportion of the Detoxifier population increased with both the initial concentration and the toxic strength of the substrate.

To address the mechanisms of how substrate toxicity affects the community assembly, we next analyzed the dynamics of intracellular and extracellular S and P concentration of the two populations. As shown in Supplementary Figure 11 , the dynamics of P largely agrees with the result derived from those non-toxic scenarios, suggesting that increasing the substrate concentration affects the amount of final product that was

exchanged between Detoxifier and Embezzler in these simulations, thus governing community assembly. Our analysis of the S dynamics clearly showed that the Detoxifier population generally maintained a lower intracellular concentration level of S than that of the Embezzler (Supplementary Figure 12), due to its conversion of S, thus possessing a growth advantage over the Embezzler population. Based on this mechanism, higher speed of the first reaction, or lower S transport rate, appears to favor the Detoxifier population since these two conditions assist Detoxifier in maintaining a lower intracellular S concentration. Consistent with this corollary, Ts_{max} was significantly positively correlated with a_1 and significantly negatively correlated with γ_s (Supplementary Table 5; Supplementary Figure 10). Overall, these results indicated that the difference in intracellular concentration of substrate is the main reason why substrate toxicity favors the Detoxifier population (Figure 1; second row).

When we assessed the community structure at different conditions of initial substrate concentration and substrate toxicity, we found that Detoxifier population are able to dominate the community when the initial substrate concentration and substrate toxicity are sufficiently high (that is, its relative proportion exceeded 50% of the community; Figure 3C; Supplementary Figure 2), suggesting that the benefit from product privatization of the Embezzler can be neutralized by higher substrate concentration and higher substrate toxicity. This phenomenon is quantitively characterized by Eqn. [2]: the maximum Detoxifier proportion in the absence of substrate toxicity (meaning $\theta = 0$), Fd_{max}, never exceed 0.5 (Supplementary Figure 9), but substrate toxicity can assist Detoxifier in breaking through this constraint, as quantified by the term $1+\frac{Ts_{max}\cdot\theta s_0}{kt+\theta s_0}$.

307 In summary, our simulations clearly showed that when a compound degradation
308 pathway is executed through MDOL in a community, both increasing substrate
309 concentration and increasing the toxicity of the substrate govern the favor the Detoxifier
310 population, thus resulting in substrate traits to govern the assembly of the community.

311 *Experimental evaluation of our rule using a liquid culture of a synthetic microbial*
312 *community engaged in MDOL*

313 To experimentally test the prediction from our ODE model, we engineered a synthetic
314 community composed of two *P. stutzeri* strains, both of which degrade an organic
315 compound, salicylate, via MDOL (Figure 4A). In this synthetic community, strain *P.*
316 *stutzeri* AN0010 only retained its ability to convert toxic substrate, salicylate [33],
317 behaving as the 'Detoxifier'; the second strain, *P. stutzeri* AN0001, was only able to
318 metabolize the intermediate catechol, but possessed the preferential access to the final
319 product, i.e., pyruvate and acetyl-CoA (Figure 4A), the direct carbon source of both
320 strains, thus behaving as the 'Embezzler'. Details about the strain construction and
321 identification are described in Supplementary Information S3. For simplicity, we
322 henceforth refer to our community as 'SMC-mdol'.

323 We first used our model to predict the assembly of SMC-mdol. We imposed the
324 experimentally measured or previous reported parameters to our ODE model
325 (Supplementary Table 6), and performed mathematical simulations across 21 different
326 toxic strength of the substrate as well as twelve different initial substrate concentration.
327 We fitted the simulation data to Eqn. [2], thus generating a predictive function that
328 matches with our synthetic system (Figure 4B). To evaluate the toxicity of salicylate,

329 we quantitively measured the relationship between strain growth rate and
330 concentrations of salicylate (see Supplementary Information S3.4 for measurement
331 details). As shown in Supplementary Figure 13, this relationship mostly follows a
332 reciprocal-form equation, and the measured dimensionless value of its toxic strength (θ)
333 was 0.0032. After inserting this value into the predictive function, we mathematically
334 predicted the effect of substrate concentration on the assembly of SMC-mdol, as
335 indicated by the red line in Figure 4B and 4C. We then cultured the SMC-mdol
336 community in liquid minimal medium supplemented with different concentrations of
337 salicylate, and analyzed the salicylate-dependent changes in structures of this synthetic
338 community. As shown in Supplementary Figure 14, the community dynamics of SMC-
339 mdol is largely consistent with the dynamics of our corresponding ODE simulations
340 (Supplementary Figure 14). In addition, the proportion of Detoxifier population
341 increased from 25.6% ± 2.5% to 61.1% ± 2.6% as a function of initial salicylate
342 concentration (Figure 4C). This shift exhibited the same trends as obtained from our
343 models, suggesting that substrate concentration governs the assembly of MDOL
344 community.
345 Importantly, when the substrate concentration reached high levels, the Detoxifier
346 population dominated the community (i.e., its relative fraction over 50 %), suggesting
347 that substrate toxicity considerably affected the assembly of the community. Moreover,
348 our predictive function accurately estimated the assembly of SMC-mdol, with a
349 predictive power (Adjusted R^2) of 0.983. Together, these experiments clearly
350 demonstrated that the assembly of microbial community engaged in MDOL can be

351 estimated by our proposed simple rules regarding concentration and toxicity of the
352 substrate.

353 **Testing the prediction in spatially structured environments**

354 In the above modeling and experiments, we investigated the assembly rules governing
355 a MDOL community, principally by assuming that the substances and cells were well-
356 mixed in the system, resulting in a spatially unstructured environment. However,
357 microorganisms are frequently observed to live in spatially structured environments,
358 such as biofilm [34-36]. Previous studies reported that different physical characteristics
359 between these two habitat types significantly affected the assembly of microbial
360 communities involved [26, 30, 37, 38]. Therefore, we set out to test whether our rule
361 derived from the assumption of a well-mixed system can be expanded to estimate the
362 assembly of a MDOL community in spatially structured environments.

363 *Individual-based modelling of the assembly of MDOL community.*

364 To develop a mathematical framework regarding the assembly of MDOL community
365 in spatially structured environment, we built an individual-based (IB) model to simulate
366 the colonization and range expansion of a MDOL community on a surface. The basic
367 configuration regarding reaction kinetics, microbial growth, and metabolic interactions
368 was identical to the framework of our ODE model. Moreover, we assumed that the
369 diffusion of S, I, and P was limited in the IB model, and mediated by their diffusion
370 coefficients (D_s , D_i, and D_p). Details about the IB model construction and simulations
371 are described in Supplementary Information S2.

372 To test our hypothesis, we ran the IB model using the parameters consistent with our

373 experimental system, but varied the toxic strength (θ) and initial concentration of the
374 substrate (s_0). We found that when toxicity was not considered and substrate
375 concentration was low (e.g., $\theta = 0$ and $S_0 = 2.5$ C-mmol/L), the model successfully
376 reproduced our hypothesis of 'Embezzler behavior'. In this case, 'Embezzler' cells
377 grew much faster than Detoxifier cells and occupied a large proportion of the available
378 space (Figure 5A; Supplementary video 1). In addition, either increasing substrate
379 concentration or introducing substrate toxicity favored the 'Detoxifier' population
380 (Figure 5A; Supplementary video 1-4). This finding is similar to our observations in
381 the spatially unstructured system, and is consistent with our two corollaries.
382 Furthermore, we found that during the colony range expansion, the two cell lineages
383 (Detoxifier and Embezzler) segregated at frontiers, forming adjacent red and green cell
384 sectors (Figure 5A; Supplementary video 1-4). Analysis of the distribution of substrate
385 and metabolites suggested that the development of this colony characteristic was mainly
386 attributed to the 'active layer effect' reported previously [28]. S is generally supplied
387 from the outside of the colony and the mass diffusion is limited, resulted in thin active
388 cell layers depending on the penetration of S, I and P (Supplementary video 1-4).
389 Consequently, community assembly in the inoculating and expanding regions may
390 follow different rules. To better quantify how community assembles in these spatially
391 structured colonies, we separately analyzed the community structures in the inoculating
392 region and expanding region of the colonies (Supplementary Figure 15). We found that
393 with the growth of colony, community structures in the inoculating region changed little,
394 while the community structures in the expanding region shifted over time, gradually

395 approaching a steady-state (Supplementary Figure 16). Therefore, we next investigated
396 how substrate traits affect the steady-state structures of the MDOL community in the
397 expanding regions.
398 As shown in Figure 5B, the community assembly in the expanding region was
399 significantly affected by substrate traits, and can be well estimated by the rule (Eqn. [2])
400 that we proposed for a spatially unstructured system. The assembly process was also
401 affected by the consuming rate of P, as it significantly affected the values of fitted
402 parameters, Fd_{max} and ks (Supplementary Figure 17; correlation analysis $p<0.0001$).
403 Further analysis suggested that increasing initial substrate concentrations assisted
404 Detoxifier to obtain more product from the environment, thus retaining higher
405 intracellular product concentrations (Supplementary Figure 18). These results indicate
406 that in spatially structured environment, substrate concentration governs the assembly
407 of MDOL community as well by affecting the amount of the final product supplying
408 from Embezzler cells to Detoxifier cells. Furthermore, we found that the Detoxifier
409 cells possessed a lower intracellular concentration level of S than that of the Embezzler
410 cells in our IB simulations (Supplementary Figure 19); higher speed of the first reaction,
411 or lower S transport rate, also significantly increased the maximum benefit (Ts_{max}) that
412 Detoxifier cells can obtained from substrate toxicity (Supplementary Figure 20;
413 correlation analysis $p<0.0001$), same as our results from ODE modelling. Therefore,
414 lower intracellular S concentration also benefits Detoxifier population when substrate
415 toxicity was taken into account in a spatially structured environment. Together, our IB
416 modelling demonstrated that the assembly of our MDOL community in spatially

417 structured environments can also be estimated by the proposed simple formula
418 governed by substrate traits.

419 *Experimental evaluation of our rule by culturing our synthetic microbial community in*
420 *spatially structured environment.*

421 We next experimentally tested whether substrate traits affect the assembly of a MDOL
422 community in spatially structured environments. Several studies have reported that type
423 IV pilus may affected the microbial colony patterns [39-41]. To directly focus on the
424 effects of substrate traits and avoid the effects of pili, we deleted the *pilA* and *pilB* genes
425 of the both strains involved in our synthetic community. This design follows other
426 studies that performed patterning experiments using non-motile strains [42-45]. The
427 derived community was named as SMC-mdol△*pilAB*. As shown in Fig. 4C, this strain
428 modification did not change the effect of substrate traits on community assembly in
429 spatially unstructured system (Figure 4C), as well as the toxic effects of salicylate on
430 the strains (Supplementary Figure 13).

431 To test our hypothesis, we cultured SMC-mdol△*pilAB* on an agarose surface to which
432 salicylate was added at different concentrations. The experimentally observed patterns
433 of the colonies were very similar to those observed for the simulated patterns (Figure
434 5C). We next separately assessed the community structures of the entire colonies, as
435 well as the inoculating region and expanding region of the colonies using image
436 analysis method. We found that, in the inoculating region, the proportion of Detoxifier
437 population slightly shifted from 40.9% ± 3.5% to 60.0% ± 6.0% (Supplementary Figure
438 21), but in the expanding region, it largely varied from 17.4% ± 1.5% to 69.0% ± 7.0%

(Figure 5D). Importantly, the experimental results of expanding region accurately fitted to our predictive function, which was derived from Eqn. [2] and IB simulations (using the same protocol as that in spatially unstructured system; Figure 5D) with a predicting power (Adjusted R^2) of 0.982. Together, our simulations and experiments demonstrated that our rules on how substrate traits govern the assembly of MDOL community were applicable even when this community grew in a spatially structured environment.

The effects of substance diffusivity on the assembly of MDOL community

Our results suggested that the effects of substrate traits on the assembly of MDOL community in spatially structured or unstructured environments can both be estimated by Eqn. [2]. However, the estimating values of the involved parameters (Fd_{max}, ks, Ts_{max}, and kt) in the predictive functions from ODE and IB model are slightly different (Figure 4 and 5), even when applying identical parameters, as well as equations to model reaction kinetics, microbial growth and metabolic interactions (Supplementary Information S2). The difference between the two predictive functions is likely to be caused by the differences in the assumptions of the two model forms. One main difference between the two models is in the mass diffusion: the IB model assumes a spatially structured environment with a limiting diffusion of S, I and P in the extracellular space, while the ODE model are constructed based on the assumptions that all the substances are rapidly and thoroughly mixed.

To eliminate the effects of other model settings and directly test whether the diffusivity of S, I and P affects the assembly of the MDOL community, we modified our IB model and performed additional simulations. We simultaneously modulated the diffusion level

461 of S, I, and P (that is, simultaneously changing D_s, D_i, and D_p), as well as constructed
462 a 'well-mixed' IB model, in which S, I and P were assumed to be evenly mixed during
463 the simulations (Supplementary Information S2.2). As shown in Fig. 6A, the predictive
464 functions derived from the scenarios with higher level of diffusivity, as well as the
465 'well-mixed' IB model, are more similar to the function derived from 'well-mixed'
466 ODE model. This result indicated that limited mass diffusion plays a significant role in
467 governing the assembly of the MDOL community.
468 How the diffusion level affects the assembly of MDOL community? Firstly, limited
469 diffusion of P promoted the product privatization by the Embezzler cells, since product
470 was distributed more around its producers when its diffusion is limited (Supplementary
471 Figure 22). From this perspective, limited diffusion of P favors the Embezzler. As
472 expected, when substrate toxicity is not considered ($\theta = 0$), the proportion of Detoxifier
473 is generally lower when the community grows in spatially structured environments
474 (Figure 6A; first row). We further tested this hypothesis by modulating the diffusion
475 level of P (solely changing D_p) in our IB model that did not include substrate toxicity.
476 As shown in Supplementary Figure 23, we found that higher level of P diffusion indeed
477 favors the Detoxifier. In conclusion, diffusivity of final product governs the assembly
478 of MDOL community by affecting the level of product privatization.
479 Secondly, Embezzler cells require intermediate metabolite I to produce final product P
480 for growth, but we found that I was largely distributed around the Detoxifier cells
481 (Supplementary Figure 24). Thus, when I diffused at a lower speed, more Detoxifier
482 cells are required to fulfill the I supply (that is, to ensure sufficient high level of I

483 concentration around Embezzler cells). Therefore, we hypothesized that limited
484 diffusion of I favored the growth of Detoxifier. As shown in Supplementary Figure 25,
485 with an increase of D_i, I was distributed more around the Embezzler cells, and the
486 relative proportion of Detoxifier cells decreases. Therefore, intermediate diffusivity
487 affects the assembly of MDOL community by influencing the efficiency of intermediate
488 exchange.

489 Finally, to investigate how substrate diffusivity affects the assembly of MDOL
490 community, we performed IB simulations initialized at different diffusion levels of the
491 substrate (solely changing D_s). As shown Figure 6A (the second row, $\theta = 0$), when
492 substrate toxicity is omitted, the proportion of Detoxifier cells increased with an
493 increase of diffusion levels of the substrate. This finding is likely to be due to the fact
494 that higher diffusion levels of S thicken the cell's 'active layer', thus increasing
495 production and secretion of the final product by Embezzler cells (Figure 6B; [45]).
496 However, limited diffusion of S will also help to maintain a lower local extracellular S
497 concentration around the Detoxifier cells (Supplementary Figure 26). When substrate
498 toxicity was taken into account, this local gradient caused the substrate toxicity to be
499 less harmful to Detoxifier cells compared to Embezzler cells. Thus, in addition to
500 thickening cell 'active layer' that benefits Detoxifier cells, higher diffusion levels of S
501 oppose the development of local substrate gradient around the Detoxifier cells.
502 Subsequently, this process also decreases the fitness of Detoxifier cells.

503 Based on our findings for the combination of these two effects, we hypothezised that
504 with the increase of substrate toxicity and its concentration, Detoxifier should gradually

505 turn to be favored in an intermediate diffusion level of substrate. This hypothesis was
506 successfully verified by our IB simulations (Figure 6A; second row. For instance, when
507 θ = 0.3 and S_0 > 10 C-mM, Detoxifier was favored at intermediate levels of D_s, 2
508 $\mu m^2/s$). We also formulated a term to estimate how the ability of the substrate to diffuse
509 affects the assembly of MDOL community, and thus obtained a new formula

510 $$DF = \frac{Fd_{max} \cdot s_0}{ks+s_0} \cdot (1+\frac{Ts_{max} \cdot \theta s_0}{kt+\theta s_0}) \cdot (\frac{s_0 D_s}{kd_1+s_0 D_s} - \frac{\theta D_s}{kd_2+\theta D_s}) \quad [3]$$

511 In this formula, $\frac{s_0 D_s}{kd_1+s_0 D_s}$ represents an estimate of the positive effect of increasing
512 substrate diffusion level via thickening cell 'active layer', which is related to the initial
513 substrate concentration (s_0; Figure 6B; [45]); $\frac{\theta D_s}{kd_2+\theta D_s}$ represents an estimate of the
514 negative effect of increasing substrate diffusion level, which is influenced by toxic
515 strength of the substrate (Figure 6A; the second row). Our fitting analysis suggested
516 that Eqn. [3] can well estimate the assembly of MDOL community in our IB simulations
517 (Figure 6C; R^2=0.994). Therefore, substrate diffusivity is another trait of substrate that
518 governs the assembly of MDOL community in spatially structured environment.
519

Discussion

Here we show how substrate traits drive the assembly of the microbial communities engaged in metabolic division of labor (MDOL) when degrading organic compounds. During this process, the population performing the first step is favored by both higher substrate concentration and its toxicity. We found that this rule is applicable both when the community grow in either a well-mixed or a spatially structured environment.

Previous studies based on meta-omics approached demonstrated that MDOL was utilized in many microbial communities specialized in degrading organic compounds[6, 46]. Inspired by these natural MDOL systems, numerous studies have recently explored strategies to divide metabolic roles across different populations in a consortium toward removal of organic pollutants[13, 47-51]. While most of these studies focused on the efficiency in pollutant degradation of these communities, a small number of studies also measured their community structures. For instance, one recent study reported that a bacterial consortium composed of *Leucobacter* sp. GP and *Achromobacter denitrificans* PR1 efficiently degrades an antibiotic, sulfamethoxazole, in which the strain GP is responsible for the initial metabolism of the sulfamethoxazole (Detoxifier), and the strain PR1 carries out the subsequent conversion (Embezzler)[17]. This study measured the structures of the community across a gradient of initial substrate concentrations, and found that the proportion of the GP is positively correlated with the initial sulfamethoxazole concentration. This observation largely agrees with the idea derived from our model and experiments, namely that increasing concentration of the substrate favors the Detoxifier population. Therefore, the proposed rule in our study

may be expanded to forecast the assembly of other communities engaged in MDOL.

Our study also compared the assembly of MDOL community when it grew in a well-mixed system and spatially structured environment. Our data indicated that limited mass diffusion in spatially structured environments is one key factor that cause the difference. This finding is reminiscent of other studies proposing that limited mass diffusion plays significant role on governing the assembly of microbial communities containing other diffusion-based interaction modes (for example, community with syntrophic exchange [30, 37, 52], community with cross-protection [53], and community with 'rock-paper-scissors' interaction [54, 55]. Here, in our study, we proved that this is also the case in the community engaged in MDOL. In addition, we reconfirmed that limited mass diffusion is one possible way to privatize public benefit [30, 37, 56]. On the one hand, it helps the Embezzler population to privatize the final product for its own growth. On the other hand, it helps the Detoxifier population to privatize its benefit from toxicant degradation (i.e., detoxification). Therefore, limited mass diffusion in spatially structured environments may be a universally used avenue for microorganisms to maintain their private benefit.

Nevertheless, our study also found that predictive function derived from the individual-based (IB) model with the assumption of mass well-mixing was not completely identical to the function from our ordinary differential equation (ODE) model, suggesting that other physical features of spatially structured environment may also contribute to the assembly of MDOL community. For example, the spatial distributions of different cell types in the colony are thought to represent another vital factor that

564 governs community assembly [27, 56-58]. In agreement with previous studies [31, 38,
565 59], our IB simulations suggested that when two populations engaged in MDOL, cells
566 from the two populations are spatially more proximal to each other than the scenario
567 when the two populations did not exhibit defined interactions (Supplementary Figure
568 27). In addition, we also found that this trait of the colony pattern (spatial proximity of
569 the two populations) was governed by substrate traits (Supplementary Figure 27).
570 Particularly, when the strength of substrate toxicity was higher, the Detoxifier cells
571 occupied the periphery of the growing colony, forming a clearly 'ring' around the
572 colony (Figure 5; Supplementary video 3; Supplementary Figure 28). The formation of
573 this ring might be due to the fact that the substrate was present at much higher
574 concentrations at the colony edge, and hence more toxic, thus largely favoring
575 Detoxifier cells. These results suggest that substrate traits also govern the spatial
576 distributions of different cells in the colony developed by MDOL community, which
577 may in turn, affect the assembly of such community. This featured cell distribution was
578 not observed in the experiments in this study, presumably because the toxicity of
579 salicylate was insufficiently high. However, one recent study found that during the
580 spatial organization of a MDOL community that collectively degrades toluene, the *P.*
581 *putida* cells responsible for the first metabolic step formed a monolayer structure in the
582 periphery of the growing colony [31]. Therefore, such cell distribution may represent a
583 critical feature of the spatial patterns developed by a MDOL community that degrades
584 substrates characterized by higher toxic strengths.
585 While our study provides critical new insights into how the community engaged in

586 MDOL assembles, a number of limitations need to be taken into consideration. First,
587 our model analysis showed that substrate toxicity is vital to govern the assembly of
588 communities engaged in MDOL. However, due to the difficulties in manipulating the
589 toxicity of the substrate (salicylate) *in vitro*, we were unable to experimentally compare
590 the impact of the different toxic strengths on community assembly. Nevertheless, our
591 model correctly predicts that simply increasing the initial substrate concentration is
592 unlikely to shape a community dominated by the Detoxifier population, while the
593 presence of substrate toxicity renders the 'Detoxifier' population in the community to
594 become dominant. Therefore, the observation that Detoxifier population was able to
595 dominate the synthetic community when high concentration of substrate was provided,
596 and the measured biotoxicity of salicylate strongly suggested that substrate toxicity
597 should be included in the assembly of the synthetic microbial community. In agreement
598 with this idea, our predictive functions involved in salicylate toxic strength fits the
599 experiment results very well. To further examine this idea, it is necessary to design a
600 better system in which the toxicity of the substrate can be modulated. For example,
601 several studies applied defined co-culturing of multiple bacterial species for degrading
602 antibiotics [17, 60, 61]. In these systems, antibiotics are toxic to all strains involved,
603 but their toxicity may be modulated by genetically modifying the expression of the
604 genes encoding the corresponding antibiotic resistance. Experiments using these well-
605 defined systems should assist in more thoroughly investigating the effects of substrate
606 toxicity on the assembly of community.
607 Second, our ODE model suggests that apart from substrate traits, five other key

parameters exist that exhibit considerable effects on the assembly of a MDOL community. Here, we primarily focused on the effects of substrate traits, without analyzing in detail how all the seven key factors collectively determine the process of community assembly. Nonetheless, our analysis presented here suggests that biotic factors such as speed of the first reaction (a_1), mass transport rate (γ_s, γ_i, γ_p), as well as consumtion rate of P (Cp), affected the assembly of the community, namely by determining the value of parameters in Eqn. [2] (i.e., Fd_{max}, ks, Ts_{max}, and kt). However, due to the difficulties in analytically solving non-linear ODEs, as well as the low efficiency of individual-based simulations [62], detailed quantitative understanding of how all these factors affect the assembly of MDOL community remains limited. We thus suggest further studies to use more simplified models that combine these elements to provide a more general description of the principles governing the assembly of a MDOL community.

To engineer stable and high-efficient microbial systems for bioproduction or biodegradation, it will be critical to predict how the communities assembled by a given set of strains exhibiting modularized functions. Our results demonstrate that, for a given community engaged in MDOL, its assembly can be quantitatively estimated from the abiotic factors, such as the traits of its substrate, suggesting that it is feasible to manage microbial communities through manipulation of specific environmental factors, to address grand challenges facing human society in agriculture, degradation of the environment, and human health.

Methods

Formulation and analyses of the ODE model

Formulation of the ODE model

To investigate the assembly of MDOL community in well-mixed system, a mathematical model was formulated using ordinary differential equations (ODEs). Here, the dimensionless forms of the models were presented. The detailed derivations of the models, and choices of parameter values are described in Supplementary Information S1.

As described in the Results section, a two-step pathway was assumed to be implemented by MDOL between two populations (Figure 2A and Figure 3A). For simplicity, the basic model was built based on five simple assumptions: (1) The systems are well mixed in each compartment (inside a cell or in the extracellular space). (2) transport of substrate (S), intermediate (I) and final product (P) is mediated by passive diffusion; (3) P was assumed to be the sole and limited resource for the growth of the two populations and its consumption was calculated following Monod equations; (4) Basic biological properties (the coefficients in Monod equations) regarding the growth of the two populations are identical, since we only focused on the effects of abiotic factors; (5) when applicable, substrate toxicity was introduced by adding three different toxic terms to the growth equation (Supplementary Table 3), dependent on intracellular S concentration of the corresponding population. The dynamics of intracellular and extracellular I and P are given by

$$\frac{ds_{1,in}}{d\tau} = -\frac{a_1}{1+s_{1,in}} s_{1,in} + \gamma_s \cdot \left(s_{out} - s_{1,in}\right) \quad [4]$$

$$\frac{ds_{2,in}}{d\tau}=\gamma_s\cdot\left(s_{out}-s_{2,in}\right) \quad [5]$$

$$\frac{di_{1,in}}{d\tau}=\frac{a_1}{1+s_{1,in}}s_{1,in}-\gamma_i\cdot\left(i_{1,in}-i_{out}\right) \quad [6]$$

$$\frac{di_{2,in}}{d\tau}=-\frac{a_2}{\beta_2+i_{2,in}}i_{2,in}+\gamma_i\cdot\left(i_{out}-i_{2,in}\right) \quad [7]$$

$$\frac{dp_{1,in}}{d\tau}=-\frac{Cp}{\beta_g+p_{1,in}}p_{1,in}+\gamma_p\cdot\left(p_{out}-p_{1,in}\right) \quad [8]$$

$$\frac{dp_{2,in}}{d\tau}=\frac{a_2}{\beta_2+i_{2,in}}i_{2,in}-\frac{Cp}{\beta_g+p_{2,in}}p_{2,in}+\gamma_p\cdot\left(p_{out}-p_{2,in}\right) \quad [9]$$

$$\frac{ds_{out}}{d\tau}=-x_1\cdot\gamma_s\cdot\left(s_{out}-s_{1,in}\right)-x_2\cdot\gamma_s\cdot\left(s_{out}-s_{2,in}\right) \quad [10]$$

$$\frac{di_{out}}{d\tau}=x_1\cdot\gamma_i\cdot\left(i_{out}-i_{1,in}\right)-x_2\cdot\gamma_i\cdot\left(i_{out}-i_{2,in}\right) \quad [11]$$

$$\frac{dp_{out}}{d\tau}=x_2\cdot\gamma_p\cdot\left(p_{out}-p_{1,in}\right)-x_1\cdot\gamma_p\cdot\left(p_{out}-p_{1,in}\right) \quad [12]$$

The growth of the two populations was modeled using a general logistic function with first-order cell death:

$$\frac{dx_1}{d\tau}=\frac{Cp}{bg+p_{1,in}}p_{1,in}yt_1x_1\left(1-\frac{x_1+x_2}{\rho}\right) \quad [13]$$

$$\frac{dx_2}{d\tau}=\frac{Cp}{bg+p_{2,in}}p_{2,in}yt_2x_2\left(1-\frac{x_1+x_2}{\rho}\right) \quad [14]$$

The definitions and dimensionless methods of all variables are listed in Supplementary Table 1. The definitions and dimensionless methods, as well as the value ranges of all the parameters involved in these equations are listed in Supplementary Table 2.

Simulation and analyzing protocol of the ODE model

Details of the simulation and analysis protocols of our ODE model and the downstream analyses are described in Supplementary Information S1.3. Briefly, to solve the community dynamics of the MDOL community with given parameter sets, numerical simulations of our ODE model were performed using *NDsolve* function of *Wolfram Mathematica*. The numerical solutions of all the variables, including the dynamics of mass (S, I, P) concentration and biomass, were recorded for further analyses. To

674 perform simulations with numerous parameter sets, as well as the downstream analysis,
675 custom *Mathematica* scripts were wrote mainly based on the *Do* loop function.

676 **Individual-based modeling**

677 Our individual based (IB) model was constructed based on *gro* platform (https:
678 https://github.com/liaupm/GRO-LIA), a simulator designed by Gutiérrez and
679 colleagues aiming to describe multicellular bacterial behavior [63]. The model aims to
680 simulate the growth of a microbial colony composed of two populations who execute
681 substrate degradation via MDOL on a surface. The model was formulated mainly using
682 the same equations as our dimensional ODE model (Supplementary Information S1.1,
683 Eqns. [S1]-[S13]) to characterize the intra- and extracellular dynamics of mass (S, I, P)
684 concentration, as well as to calculate the rate of cell growth. Four main differences exist
685 between our IB model and the ODE model: (1) The IB model was formulated on a
686 spatially structured surface, and the diffusion of S, I, and P was limited; (2) Mass
687 dynamics was modelled at single-cell level; (3) The growth of both populations was
688 modelled at single-cell level, and passive cell shoving during the cell growth was
689 included; (4) cells were inoculated in the center of the surface, and the entire community
690 underwent 'colony range expansion', a process whereby the community immigrate
691 outwards as a whole, driven by the force generated from cell growth and division
692 (Supplementary Figure 15). The mathematical framework formulating these four points
693 is described in Supplementary Information S2.1. To implement our design of the IB
694 model, custom codes were written in *gro* language. Variables and Parameters in the IB
695 model are summarized in Supplementary Table 7. Details of the IB simulation

696 workflow are described in Supplementary Information S2.

697 **Experimental verification of our model prediction**

698 *Genetic manipulation of the P. stutzeri strains*

699 All *P. stutzeri* strains were engineered from a naphthalene-degrading bacterial strain *P.*
700 *stutzeri* AN10 [64]. Genes that encode the key enzymes responsible for corresponding
701 metabolic steps in salicylate degradation pathway were knocked out to generate the *P.*
702 *stutzeri* strains. The details of the genetic manipulation of are described in
703 Supplementary information S3.

704 *Liquid cultivation of our synthetic microbial communities*

705 Liquid cultivation of our synthetic microbial communities was performed in 96-well
706 plates that contains 120 μL fresh minimum medium. Proportions of the two populations
707 in the community were estimated by measuring the fluorescent intensity of the two
708 strains involved using a microplate reader (Molecular Devices, Sunnyvale, America).
709 Detailed protocols are described in Supplementary information S4.

710 *Colony pattern formation assays*

711 Colony pattern formation assays were performed on the agarose surface in a Petri dish
712 (60 mm in diameter). Images of the colony patterns were taken under a 5× objective
713 using a Leica DM6000B fluorescence microscope (Leica Corporation, Wetzlar,
714 Germany) equipped with a LED fluorescence illuminator (Leica Corporation). The
715 relative fraction of each population in the colonies was measured by image analysis, as
716 well as similar fluorescence-measurement method as performed in liquid cultivation
717 experiments. Detailed protocols are described in Supplementary information S5.

718 **Statistical analysis**

719 Unless indicated otherwise, the number of replicates was three for each simulation, and
720 six for each experiment. For comparative statistics, unpaired, two-tailed, Student's t-
721 test was performed in Wolfram Mathematica (version 12.4). To fit the data to the
722 proposed function, Nonlinearmodelfit function of the Wolfram Mathematica (version
723 12.4) was applied.

724 **Code availability**

725 All custom *Mathematica* codes used for ODE simulation and data analyses, as well as
726 the source *gro* codes used for our IB simulations are available at Github:
727 https://github.com/RoyWang1991/MDOLcode/tree/master/MDOL-spatial.

728 **Competing Interests**

729 The authors declare that they have no conflict of interest.

730 **Acknowledgments**

731 We wish to thank Professor Ping Xu (Shanghai Jiao Tong University, Shanghai, P.R.
732 China) for supplying plasmid pMMPc-Gm, used for fluorescence labeling in this study;
733 Dr. Min Lin (Chinese Academy of Agricultural Sciences, Beijing, P.R. China) for
734 providing plasmid pK18mobsacB and pRK2013, used for genetic engineering in this
735 work; Professor Martin Ackermann (ETH Zurich, Zurich, Switzerland), Dr. David
736 Johnson (Eawag, Dübendorf, Switzerland) and Yinyin Ma (Eawag, Dübendorf,
737 Switzerland) for constructive inputs on the design of this study; Professor Martín
738 Gutiérrez (Universidad Politécnica de Madrid, Madrid, Spain) for his kindly guidance
739 for the set-up of the *gro* platform for the individual-based simulations; Dr. T. Juelich

(UCAS, Beijing) for linguistic assistance during the preparation of this manuscript. This work was supported by National Key R&D Program of China (2018YFA0902100 and 2018YFA0902103), and National Natural Science Foundation of China (91951204, 31761133006, 31770120, and 31770118).

745 **References**

746 1. Kreft JU, Griffin BM, Gonzalez-Cabaleiro R. Evolutionary causes and consequences
747 of metabolic division of labour: why anaerobes do and aerobes don't. Curr Opin
748 Biotechnol. 2020;62:80-7; doi:10.1016/j.copbio.2019.08.008.

749 2. Tsoi R, Wu F, Zhang C, Bewick S, Karig D, You L. Metabolic division of labor in
750 microbial systems. Proc Natl Acad Sci U S A. 2018;115:10:2526-31;
751 doi:10.1073/pnas.1716888115.

752 3. Harvey E, Heys J, Gedeon T. Quantifying the effects of the division of labor in
753 metabolic pathways. J Theor Biol. 2014;360:222-42; doi:10.1016/j.jtbi.2014.07.011.

754 4. Thommes M, Wang T, Zhao Q, Paschalidis IC, Segre D. Designing Metabolic
755 Division of Labor in Microbial Communities. mSystems. 2019;4:2;
756 doi:10.1128/mSystems.00263-18.

757 5. Seelke R. The Prokaryotes: a handbook on the biology of bacteria. Choice: Current
758 Reviews for Academic Libraries. 2007;45:1:68-.

759 6. Dombrowski N, Donaho JA, Gutierrez T, Seitz KW, Teske AP, Baker BJ.
760 Reconstructing metabolic pathways of hydrocarbon-degrading bacteria from the
761 Deepwater Horizon oil spill. Nat Microbiol. 2016;1:7:16057;
762 doi:10.1038/nmicrobiol.2016.57.

763 7. West SA, Cooper GA. Division of labour in microorganisms: an evolutionary
764 perspective. Nat Rev Microbiol. 2016;14:11:716-23; doi:10.1038/nrmicro.2016.111.

765 8. van Gestel J, Vlamakis H, Kolter R. Division of Labor in Biofilms: the Ecology of
766 Cell Differentiation. Microbiol Spectr. 2015;3:2:MB-0002-2014;

767 doi:10.1128/microbiolspec.MB-0002-2014.

768 9. Lilja EE, Johnson DR. Segregating metabolic processes into different microbial cells
769 accelerates the consumption of inhibitory substrates. Isme Journal. 2016;10:7:1568-78;
770 doi:10.1038/ismej.2015.243.

771 10. Schink B, Pfennig N. Fermentation of Trihydroxybenzenes by Pelobacter-
772 Acidigallici Gen-Nov Sp-Nov a New Strictly Anaerobic, Non-Sporeforming Bacterium.
773 Arch Microbiol. 1982;133:3:195-201; doi:Doi 10.1007/Bf00415000.

774 11. Wang CY, Huang Y, Zhang ZT, Hao H, Wang H. Absence of the nahG-like gene
775 caused the syntrophic interaction between *Marinobacter* and other microbes in PAH-
776 degrading process. J Hazard Mater. 2020;384; doi:ARTN 121387
777 10.1016/j.jhazmat.2019.121387.

778 12. Katsuyama C, Nakaoka S, Takeuchi Y, Tago K, Hayatsu M, Kato K.
779 Complementary cooperation between two syntrophic bacteria in pesticide degradation.
780 Journal of Theoretical Biology. 2009;256:4:644-54; doi:10.1016/j.jtbi.2008.10.024.

781 13. Yang C, Li Y, Zhang K, Wang X, Ma C, Tang H, Xu P. Atrazine degradation by a
782 simple consortium of *Klebsiella* sp. A1 and *Comamonas* sp. A2 in nitrogen enriched
783 medium. Biodegradation. 2010;21:1:97-105; doi:10.1007/s10532-009-9284-9.

784 14. Billet L, Devers M, Rouard N, Martin-Laurent F, Spor A. Labour sharing promotes
785 coexistence in atrazine degrading bacterial communities. Sci Rep. 2019;9:1:18363;
786 doi:10.1038/s41598-019-54978-2.

787 15. Gilbert ES, Walker AW, Keasling JD. A constructed microbial consortium for
788 biodegradation of the organophosphorus insecticide parathion. Appl Microbiol Biot.

789 2003;61:1:77-81; doi:10.1007/s00253-002-1203-5.

790 16. Meyer-Cifuentes IE, Werner J, Jehmlich N, Will SE, Neumann-Schaal M, Ozturk
791 B. Synergistic biodegradation of aromatic-aliphatic copolyester plastic by a marine
792 microbial consortium. Nature Communications. 2020;11:1; doi:ARTN
793 579010.1038/s41467-020-19583-2.

794 17. Reis AC, Cvancarova M, Liu Y, Lenz M, Hettich T, Kolvenbach BA, Corvini PFX,
795 Nunes OC. Biodegradation of sulfamethoxazole by a bacterial consortium of
796 *Achromobacter denitrificans* PR1 and *Leucobacter* sp GP. Appl Microbiol Biot.
797 2018;102:23:10299-314; doi:10.1007/s00253-018-9411-9.

798 18. Peng XF, Wilken S, Lankiewicz TS, Gilmore SP, Brown JL, Henske JK, Swift CL,
799 Salamov A, Barry K, Grigoriev IV, Theodorou MK, Valentine DL, O'Malley MA.
800 Genomic and functional analyses of fungal and bacterial consortia that enable
801 lignocellulose breakdown in goat gut microbiomes. Nat Microbiol. 2021;6:4:499-+;
802 doi:10.1038/s41564-020-00861-0.

803 19. Kato S, Haruta S, Cui ZJ, Ishii M, Igarashi Y. Stable coexistence of five bacterial
804 strains as a cellulose-degrading community. Appl Environ Microb. 2005;71:11:7099-
805 106; doi:10.1128/Aem.71.11.7099-7106.2005.

806 20. Koudryashova Y, Chizhova T, Tishchenko P, Hayakawa K. Seasonal Variability of
807 Polycyclic Aromatic Hydrocarbons (PAHs) in a Coastal Marine Area in the
808 Northwestern Region of the Sea of Japan/East Sea (Possiet Bay). Ocean Sci J.
809 2019;54:4:635-55; doi:10.1007/s12601-019-0031-9.

810 21. Jiang Y, Hu X, Yves UJ, Zhan H, Wu Y. Status, source and health risk assessment

811 of polycyclic aromatic hydrocarbons in street dust of an industrial city, NW China.
812 Ecotoxicol Environ Saf. 2014;106:11-8; doi:10.1016/j.ecoenv.2014.04.031.
813 22. Ozaki N, Takamura Y, Kojima K, Kindaichi T. Loading and removal of PAHs in a
814 wastewater treatment plant in a separated sewer system. Water Res. 2015;80:337-45;
815 doi:10.1016/j.watres.2015.05.002.
816 23. Peng RH, Xiong AS, Xue Y, Fu XY, Gao F, Zhao W, Tian YS, Yao QH. Microbial
817 biodegradation of polyaromatic hydrocarbons. Fems Microbiol Rev. 2008;32:6:927-55;
818 doi:10.1111/j.1574-6976.2008.00127.x.
819 24. Park W, Jeon CO, Cadillo H, DeRito C, Madsen EL. Survival of naphthalene-
820 degrading Pseudomonas putida NCIB 9816-4 in naphthalene-amended soils: toxicity
821 of naphthalene and its metabolites. Appl Microbiol Biot. 2004;64:3:429-35;
822 doi:10.1007/s00253-003-1420-6.
823 25. Hall-Stoodley L, Costerton JW, Stoodley P. Bacterial biofilms: from the natural
824 environment to infectious diseases. Nat Rev Microbiol. 2004;2:2:95-108;
825 doi:10.1038/nrmicro821.
826 26. Nadell CD, Drescher K, Foster KR. Spatial structure, cooperation and competition
827 in biofilms. Nat Rev Microbiol. 2016;14:9:589-600; doi:10.1038/nrmicro.2016.84.
828 27. Dal Co A, van Vliet S, Kiviet DJ, Schlegel S, Ackermann M. Short-range
829 interactions govern the dynamics and functions of microbial communities. Nat Ecol
830 Evol. 2020;4:3:366-75; doi:10.1038/s41559-019-1080-2.
831 28. Nadell CD, Foster KR, Xavier JB. Emergence of Spatial Structure in Cell Groups
832 and the Evolution of Cooperation. Plos Computational Biology. 2010;6:3; doi:ARTN

833 e100071610.1371/journal.pcbi.1000716.

834 29. Frost I, Smith WPJ, Mitri S, San Millan A, Davit Y, Osborne JM, Pitt-Francis JM,
835 MacLean RC, Foster KR. Cooperation, competition and antibiotic resistance in
836 bacterial colonies. Isme Journal. 2018;12:6:1582-93; doi:10.1038/s41396-018-0090-4.

837 30. Momeni B, Waite AJ, Shou W. Spatial self-organization favors heterotypic
838 cooperation over cheating. Elife. 2013;2:e00960; doi:10.7554/eLife.00960.

839 31. Tecon R, Or D. Cooperation in carbon source degradation shapes spatial self-
840 organization of microbial consortia on hydrated surfaces. Sci Rep-Uk. 2017;7;
841 doi:ARTN 4372610.1038/srep43726.

842 32. Quintas C, Leyva JS, Sotoca R, Loureiro-Dias MC, Peinado JM. A model of the
843 specific growth rate inhibition by weak acids in yeasts based on energy requirements.
844 Int J Food Microbiol. 2005;100:1-3:125-30; doi:10.1016/j.ijfoodmicro.2004.10.009.

845 33. Lanfranconi MP, Christie-Oleza JA, Martin-Cardona C, Suarez-Suarez LY, Lalucat
846 J, Nogales B, Bosch R. Physiological role of NahW, the additional salicylate
847 hydroxylase found in *Pseudomonas stutzeri* AN10. Fems Microbiol Lett.
848 2009;300:2:265-72; doi:10.1111/j.1574-6968.2009.01787.x.

849 34. Nadell CD, Drescher K, Foster KR. Spatial structure, cooperation and competition
850 in biofilms. Nat Rev Microbiol. 2016;14:9:589-600; doi:10.1038/nrmicro.2016.84.

851 35. Mitri S, Xavier JB, Foster KR. Social evolution in multispecies biofilms. P Natl
852 Acad Sci USA. 2011;108:10839-46; doi:10.1073/pnas.1100292108.

853 36. Xavier JB, Foster KR. Cooperation and conflict in microbial biofilms. P Natl Acad
854 Sci USA. 2007;104:3:876-81; doi:10.1073/pnas.0607651104.

855 37. Pande S, Kaftan F, Lang S, Svatos A, Germerodt S, Kost C. Privatization of
856 cooperative benefits stabilizes mutualistic cross-feeding interactions in spatially
857 structured environments. ISME J. 2016;10:6:1413-23; doi:10.1038/ismej.2015.212.
858 38. Goldschmidt F, Regoes RR, Johnson DR. Successive range expansion promotes
859 diversity and accelerates evolution in spatially structured microbial populations. Isme
860 Journal. 2017;11:9:2112-23; doi:10.1038/ismej.2017.76.
861 39. Klausen M, Heydorn A, Ragas P, Lambertsen L, Aaes-Jorgensen A, Molin S, Tolker-
862 Nielsen T. Biofilm formation by *Pseudomonas aeruginosa* wild type, flagella and type
863 IV pili mutants. Mol Microbiol. 2003;48:6:1511-24; doi:10.1046/j.1365-
864 2958.2003.03525.x.
865 40. Barken KB, Pamp SJ, Yang L, Gjermansen M, Bertrand JJ, Klausen M, Givskov M,
866 Whitchurch CB, Engel JN, Tolker-Nielsen T. Roles of type IV pili, flagellum-mediated
867 motility and extracellular DNA in the formation of mature multicellular structures in
868 *Pseudomonas aeruginosa* biofilms. Environ Microbiol. 2008;10:9:2331-43;
869 doi:10.1111/j.1462-2920.2008.01658.x.
870 41. O'Toole GA, Kolter R. Flagellar and twitching motility are necessary for
871 *Pseudomonas aeruginosa* biofilm development. Mol Microbiol. 1998;30:2:295-304;
872 doi:10.1046/j.1365-2958.1998.01062.x.
873 42. Hallatschek O, Hersen P, Ramanathan S, Nelson DR. Genetic drift at expanding
874 frontiers promotes gene segregation. P Natl Acad Sci USA. 2007;104:50:19926-30;
875 doi:10.1073/pnas.0710150104.
876 43. Hallatschek O, Nelson DR. Life at the Front of an Expanding Population. Evolution.

877 2010;64:1:193-206; doi:10.1111/j.1558-5646.2009.00809.x.

878 44. Korolev KS, Xavier JB, Nelson DR, Foster KR. A Quantitative Test of Population
879 Genetics Using Spatiogenetic Patterns in Bacterial Colonies. American Naturalist.
880 2011;178:4:538-52; doi:10.1086/661897.

881 45. Mitri S, Clarke E, Foster KR. Resource limitation drives spatial organization in
882 microbial groups. Isme Journal. 2016;10:6:1471-82; doi:10.1038/ismej.2015.208.

883 46. Yu K, Yi S, Li B, Guo F, Peng X, Wang Z, Wu Y, Alvarez-Cohen L, Zhang T. An
884 integrated meta-omics approach reveals substrates involved in synergistic interactions
885 in a bisphenol A (BPA)-degrading microbial community. Microbiome. 2019;7:1:16;
886 doi:10.1186/s40168-019-0634-5.

887 47. Li Z, Yoshida N, Wang A, Nan J, Liang B, Zhang C, Zhang D, Suzuki D, Zhou X,
888 Xiao Z, Katayama A. Anaerobic mineralization of 2,4,6-tribromophenol to CO2 by a
889 synthetic microbial community comprising *Clostridium*, *Dehalobacter*, and
890 *Desulfatiglans*. Bioresour Technol. 2015;176:225-32;
891 doi:10.1016/j.biortech.2014.10.097.

892 48. Che S, Men Y. Synthetic microbial consortia for biosynthesis and biodegradation:
893 promises and challenges. J Ind Microbiol Biotechnol. 2019;46:9-10:1343-58;
894 doi:10.1007/s10295-019-02211-4.

895 49. Hudcova T, Halecky M, Kozliak E, Stiborova M, Paca J. Aerobic degradation of
896 2,4-dinitrotoluene by individual bacterial strains and defined mixed population in
897 submerged cultures. J Hazard Mater. 2011;192:2:605-13;
898 doi:10.1016/j.jhazmat.2011.05.061.

899 50. Roell GW, Zha J, Carr RR, Koffas MA, Fong SS, Tang YJ. Engineering microbial
900 consortia by division of labor. Microb Cell Fact. 2019;18:1:35; doi:10.1186/s12934-
901 019-1083-3.
902 51. Jia XQ, He Y, Jiang DW, Liu C, Lu WY. Construction and analysis of an engineered
903 *Escherichia coli-Pseudomonas aeruginosa* co-culture consortium for phenanthrene
904 bioremoval. Biochem Eng J. 2019;148:214-23; doi:10.1016/j.bej.2019.05.010.
905 52. Momeni B, Brileya KA, Fields MW, Shou WY. Strong inter-population cooperation
906 leads to partner intermixing in microbial communities. Elife. 2013;2; doi:ARTN
907 e0023010.7554/eLife.00230.
908 53. Frost I, Smith WPJ, Mitri S, Millan AS, Davit Y, Osborne JM, Pitt-Francis JM,
909 MacLean RC, Foster KR. Cooperation, competition and antibiotic resistance in
910 bacterial colonies. ISME J. 2018;12:6:1582-93; doi:10.1038/s41396-018-0090-4.
911 54. Kerr B, Riley MA, Feldman MW, Bohannan BJ. Local dispersal promotes
912 biodiversity in a real-life game of rock-paper-scissors. Nature. 2002;418:6894:171-4;
913 doi:10.1038/nature00823.
914 55. Nahum JR, Harding BN, Kerr B. Evolution of restraint in a structured rock-paper-
915 scissors community. P Natl Acad Sci USA. 2011;108:10831-8;
916 doi:10.1073/pnas.1100296108.
917 56. Wang M, Liu X, Nie Y, Wu XL. Selfishness driving reductive evolution shapes
918 interdependent patterns in spatially structured microbial communities. ISME J.
919 2021;15:5:1387-401; doi:10.1038/s41396-020-00858-x.
920 57. Kim W, Racimo F, Schluter J, Levy SB, Foster KR. Importance of positioning for

921 microbial evolution. Proc Natl Acad Sci U S A. 2014;111:16:E1639-47;
922 doi:10.1073/pnas.1323632111.
923 58. Liu X, Wang M, Nie Y, Wu X-L. Successful microbial colonization of space using
924 an anti-aggregation strategy. bioRxiv. 2021:2021.07.09.451734;
925 doi:10.1101/2021.07.09.451734.
926 59. Goldschmidt F, Regoes RR, Johnson DR. Metabolite toxicity slows local diversity
927 loss during expansion of a microbial cross-feeding community. Isme Journal.
928 2018;12:1:136-44; doi:10.1038/ismej.2017.147.
929 60. Liu CX, Xu QM, Yu SC, Cheng JS, Yuan YJ. Bio-removal of tetracycline antibiotics
930 under the consortium with probiotics *Bacillus clausii* T and *Bacillus amyloliquefaciens*
931 producing biosurfactants. Sci Total Environ. 2020;710; doi:ARTN
932 13632910.1016/j.scitotenv.2019.136329.
933 61. Kong XX, Jiang JL, Qiao B, Liu H, Cheng JS, Yuan YJ. The biodegradation of
934 cefuroxime, cefotaxime and cefpirome by the synthetic consortium with probiotic
935 Bacillus clausii and investigation of their potential biodegradation pathways. Sci Total
936 Environ. 2019;651:271-80; doi:10.1016/j.scitotenv.2018.09.187.
937 62. Hellweger FL, Clegg RJ, Clark JR, Plugge CM, Kreft JU. Advancing microbial
938 sciences by individual-based modelling. Nat Rev Microbiol. 2016;14:7:461-71;
939 doi:10.1038/nrmicro.2016.62.
940 63. Gutierrez M, Gregorio-Godoy P, Perez Del Pulgar G, Munoz LE, Saez S,
941 Rodriguez-Paton A. A New Improved and Extended Version of the Multicell Bacterial
942 Simulator gro. ACS Synth Biol. 2017;6:8:1496-508; doi:10.1021/acssynbio.7b00003.

943 64. Brunet-Galmes I, Busquets A, Pena A, Gomila M, Nogales B, Garcia-Valdes E,
944 Lalucat J, Bennasar A, Bosch R. Complete Genome Sequence of the Naphthalene-
945 Degrading Bacterium *Pseudomonas stutzeri* AN10 (CCUG 29243). J Bacteriol.
946 2012;194:23:6642-3; doi:10.1128/Jb.01753-12.
947

948 **Figures**

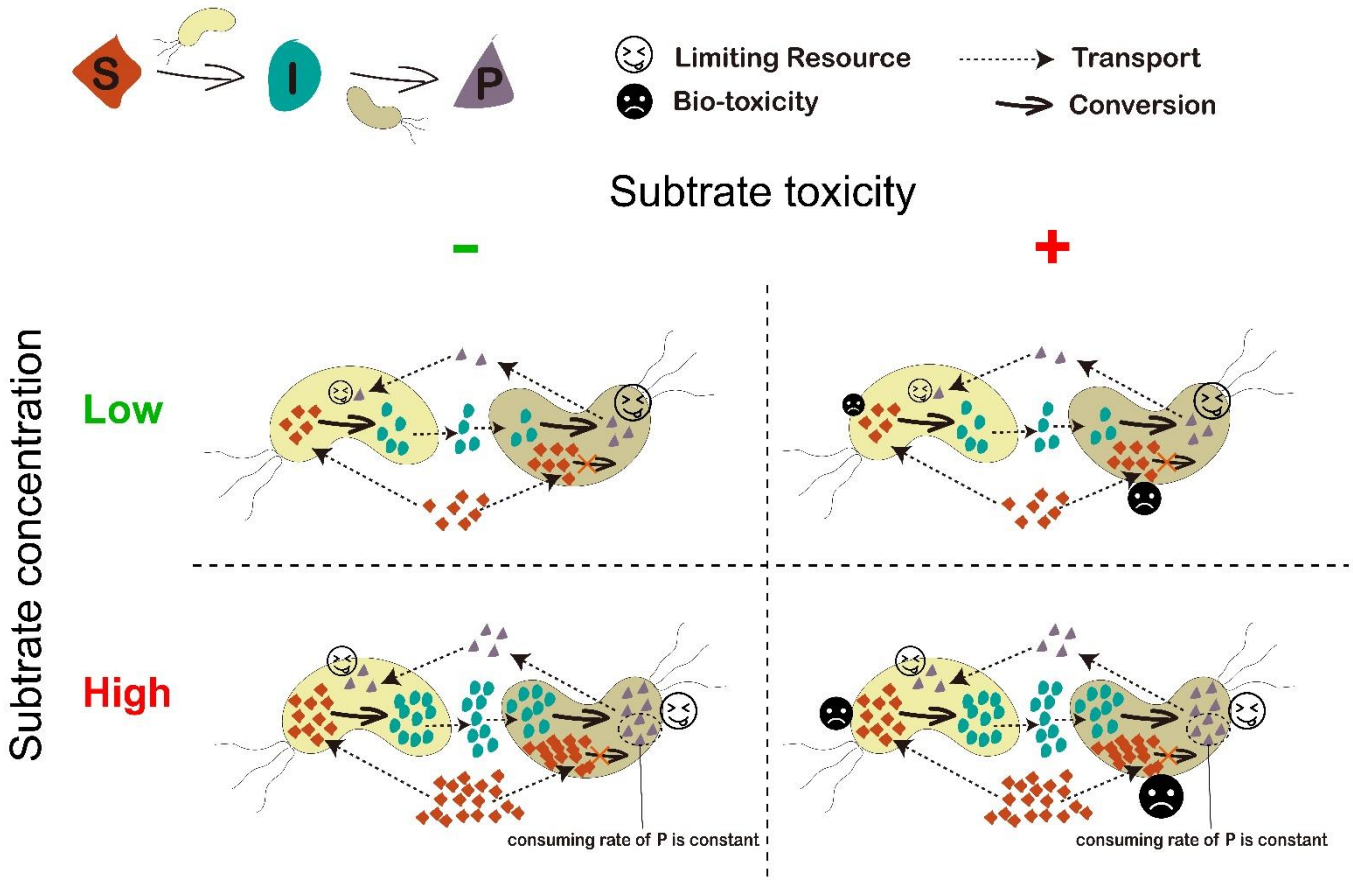

949

950 **Figure 1** Hypothesis for how substrate concentration and toxicity govern the assembly of community engaged in MDOL. In a community

951 degrading an organic compound through metabolic division of labor (MDOL), final product was assumed to be the sole resource and was
952 synthesized by the strain performing the second step. Therefore, this strain will obtain more nutrients (denoted as bigger ‘smiling face’), while the
953 other strain has to collect product released from this population (denoted as smaller ‘smiling face’). Thus, the last population was named
954 ‘Embezzler’. However, increasing the concentration of the substrate (vertical axis) improves the flux of the pathway. Since the P consuming ability
955 of Embezzler cells is limited (dashed box), increasing the concentration will lead to higher final product leakiness, favoring the growth of the first
956 population. Moreover, introducing substrate biotoxicity (horizontal axis) also favors the first population, because it converts this toxic substrate
957 (denoted as smaller sad face), resulting in lower intracellular substrate concentration compared to that of the Embezzler cells (denoted as bigger
958 sad face). Thus, the first population was named ‘Detoxifier’.

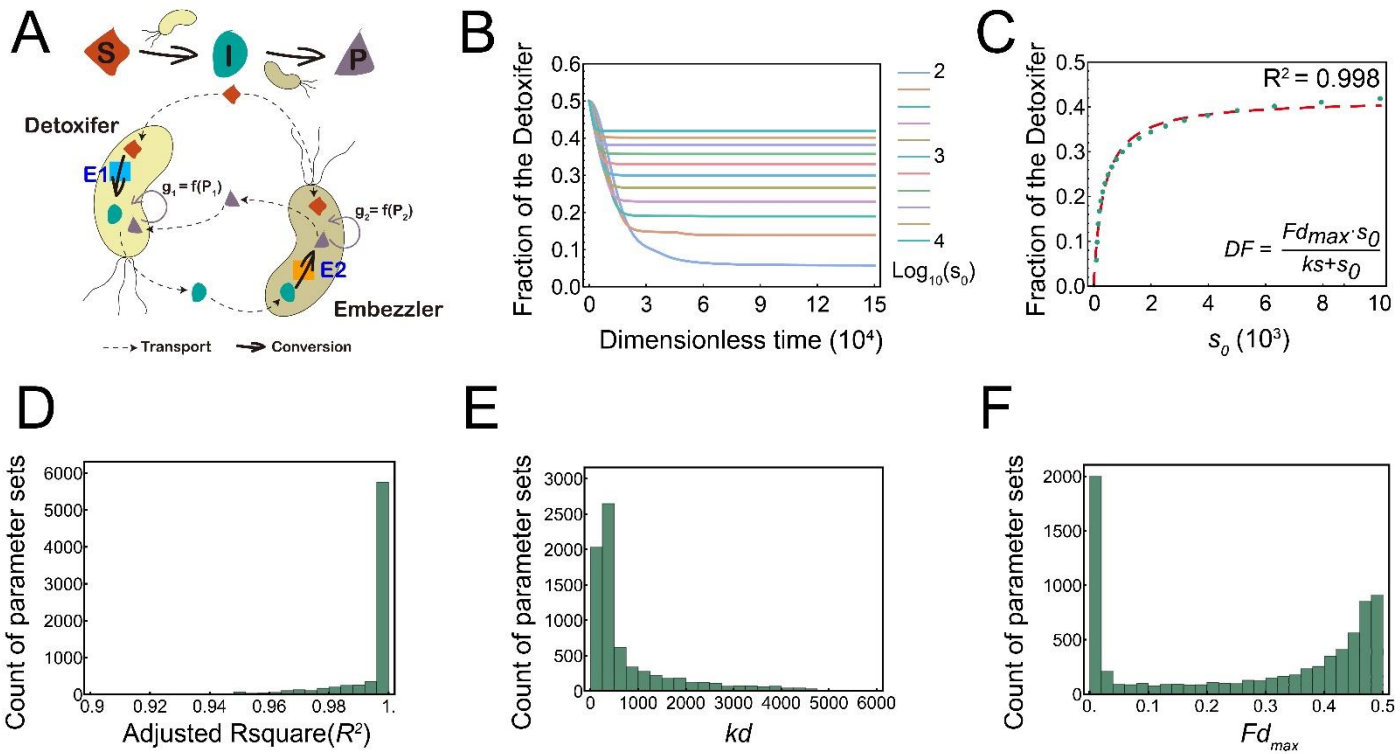

Figure 2 Simulation of the ordinary differential equation (ODE) model excluding substrate toxicity. (A) Schematic diagram showing the basic assumptions of our ODE model without including substrate toxicity. (B-C) A representative case shows how substrate concentration affects the assembly of our? a? MDOL community. The simulation dynamics of the fraction of Detoxifier population with the conditions of different initial substrate concentrations are shown in (B). The relationship between substrate concentration and stead-state fraction of Detoxifier is shown in (C).

964 In (C), the green dots denote the simulated stead-state fraction of Detoxifier, and the red dashed line shows the plot of the best fitting function

965 using Eqn. [1]. Parameter values used in these simulations: $y = 10^{-4}$, $Cp = 10$, $bg = 1$, $a_1 = 10000$, $a_2 = 1000$, $\beta_2 = 1$, $\gamma_s = 1$, $\gamma_i = 1$, $\gamma_p = 1$, $\rho = 10^{-2}$.

966 The best fitting value of ks in this case is 35.3, and that of Fd_{max} is 0.417. (D-F) Distributions of Adjusted R^2 (D) of the fitting functions, best fitting

967 value of ks (E) and Fd_{max} (F) in the second-round simulations that does not include substrate toxicity, using 7776 parameter value combinations of

968 the five key parameters (a_1, γ_s, γ_i, γ_p, and Cp).

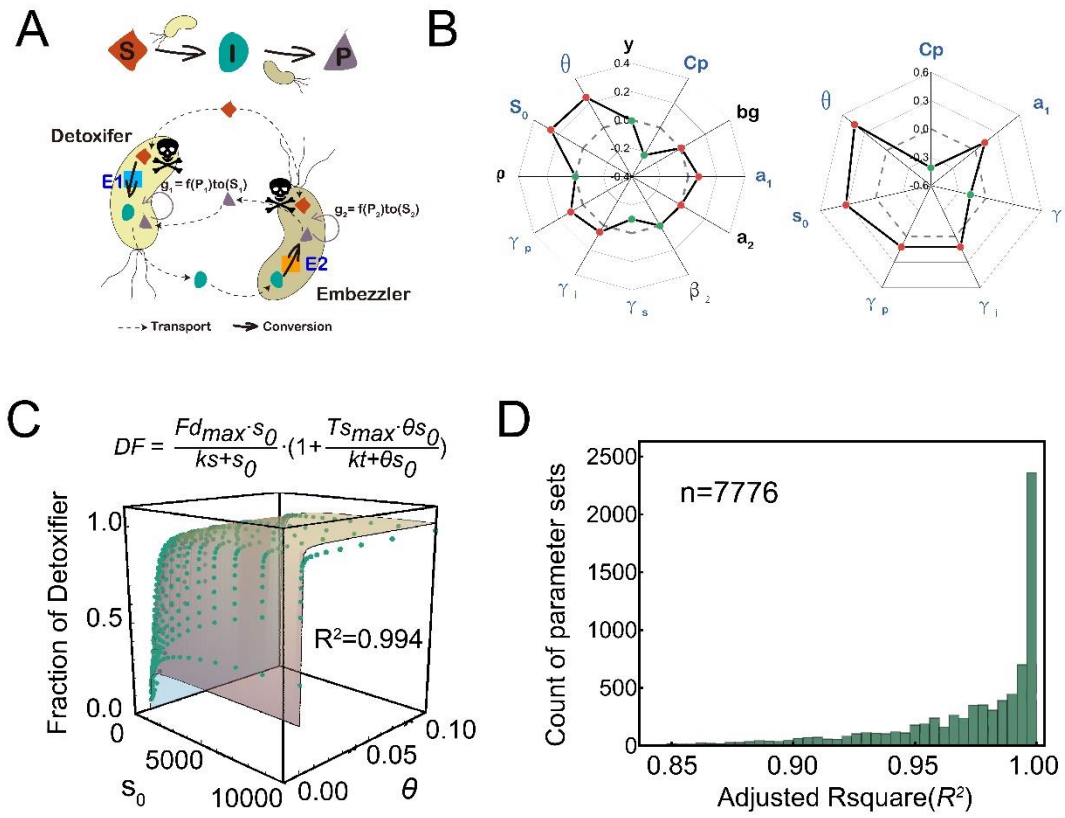

Figure 3 Simulation of the ordinary differential equation (ODE) model that includes substrate toxicity, suggesting that both substrate concentration and its toxicity collectively affect the assembly of a community engaged in MDOL. (A) Schematic diagram showing the basic assumptions of our ODE model that includes substrate toxicity. (B) Multiple linear regression analysis of the simulation results of the ODE model showed how the parameters included in the model affect the assembly of the MDOL community. Left: results from the first-round simulations that considered all the twelve parameters are shown. Blue font denotes the identified key parameters. Right: results from the second-round simulations that only considered the seven key parameters. The axis of the radar plot denotes the values of fitting coefficients of the parameters from multiple linear regression analyses. Red dots denote the steady-state

fraction of Detoxifier is positively correlated with corresponding parameter, while the green dots represent the negative correlation. The origin axis (0) is highlighted by dash line to emphasize the fact that the closer a value is to zero, the smaller the effect on the community assembly of the corresponding parameter. The data are also listed in Supplementary Table 4 and Supplementary Table 5. In this analysis, the toxic effects of substrate on population growth were assumed to follow a reciprocal relationship. Results considering other relationships are shown in Supplementary Figure 3. (C) A representative case shows how both substrate concentration and its toxicity collectively affect the stead-state proportion of Detoxifier cells. The green dots denote the simulated stead-state fraction of Detoxifier, and the surface shows the plot of the best fitting function using Eqn. [2]. Parameter values used in these simulations: $y = 10^{-4}$, $Cp = 10$, $bg = 1$, $a_1 = 10000$, $a_2 = 1000$, $\beta_2 = 1$, $\gamma_s = 1$, $\gamma_i = 1$, $\gamma_p = 1$, $\rho = 10^{-2}$. The best fitting value of ks, Fd_{max}, kt, and TS_{max} in this case are 48.9, 0.423, 0.848, 3.39, respectively. (D) Distributions of Adjusted R^2 of the fitting functions in the second-round simulations that includes substrate toxicity, using 7776 parameter value combinations of the five key parameters (a_1, γ_s, γ_i, γ_p, and Cp).

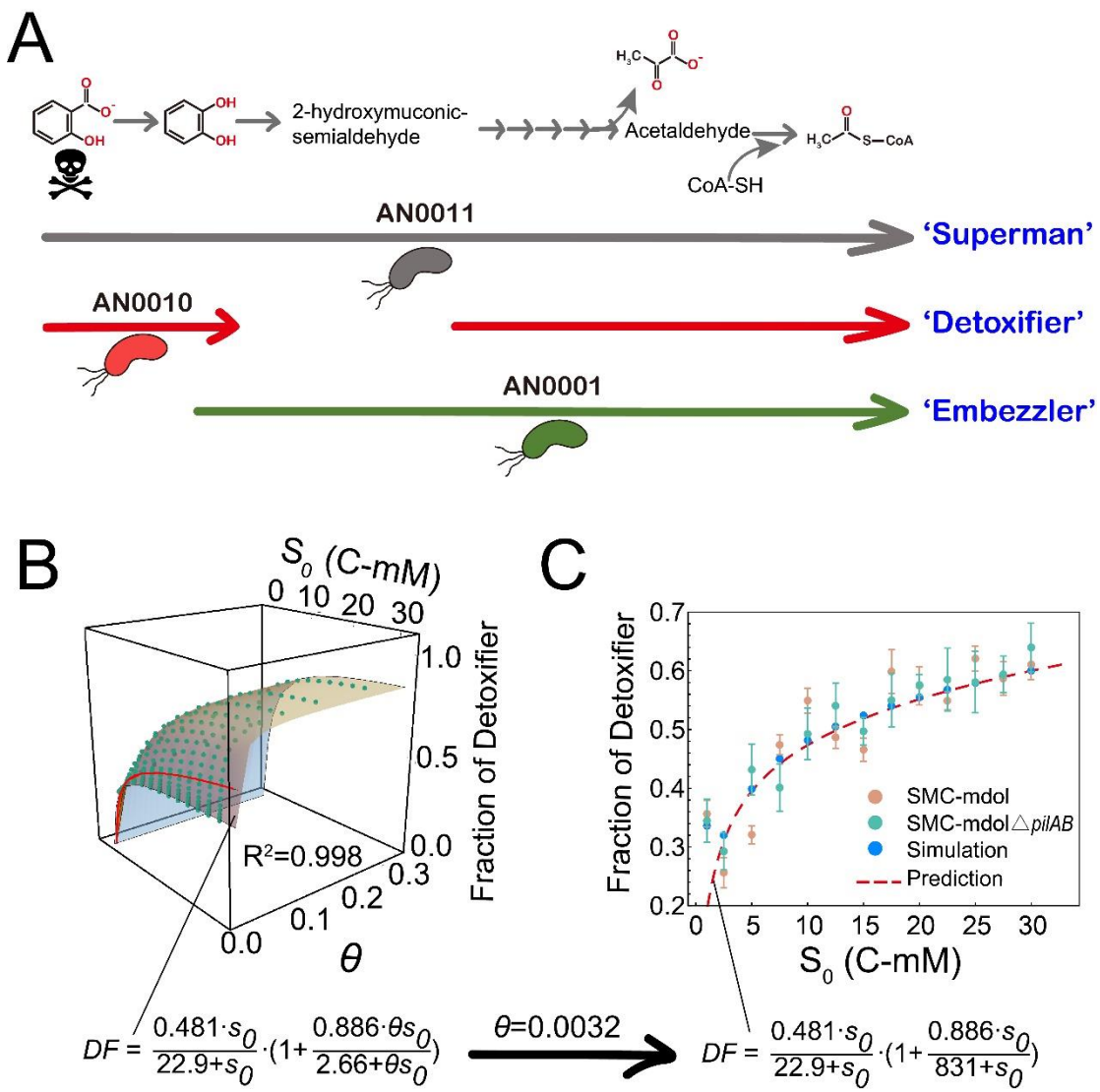

Figure 4 Community assembly of SMC-mdol in a spatially unstructured system across different substrate traits. (A) Design of the SMC-mdol. Shown are the pathway of salicylate degradation in 'Superman' strain *P. stutzeri* AN0011, as well as partial pathways carried out by Detoxifier strain AN0010 and Embezzler strain AN0001. Skull marks that salicylate is toxic. (B) Predicting the assembly of the synthetic community using our ODE model, as well as the derived predictive function using Eqn. [2]. The relationship between the steady-state fraction of the Detoxifier population and substrate concentration (s_0), as well as substrate toxic strength (θ), was built from our mathematical model using parameters consistent with our experiemental system. Each

green dot shows the steady-state fraction of Detoxifier obtained by one simulation accociated with the specific parameter set. The surface diagram shows distribution of the steady-state fraction of Detoxifier predicted by our proposed simple formula. The Red line in the surface denotes the scenarios θ=0.0032, which is the toxic strength of salicylate obtained from experiemental measurements. (C) The experimental measured steady-state fractions of Detoxifier in cultures with different salicylate concentrations is consistent with those from mathematical predictions. Note that in the plots, substrate concentrations are shown in dimentional form (S_0, Cmmol/L), but in the predictive functions, the fitting analysis was performed using its dimensionless form (s_0).

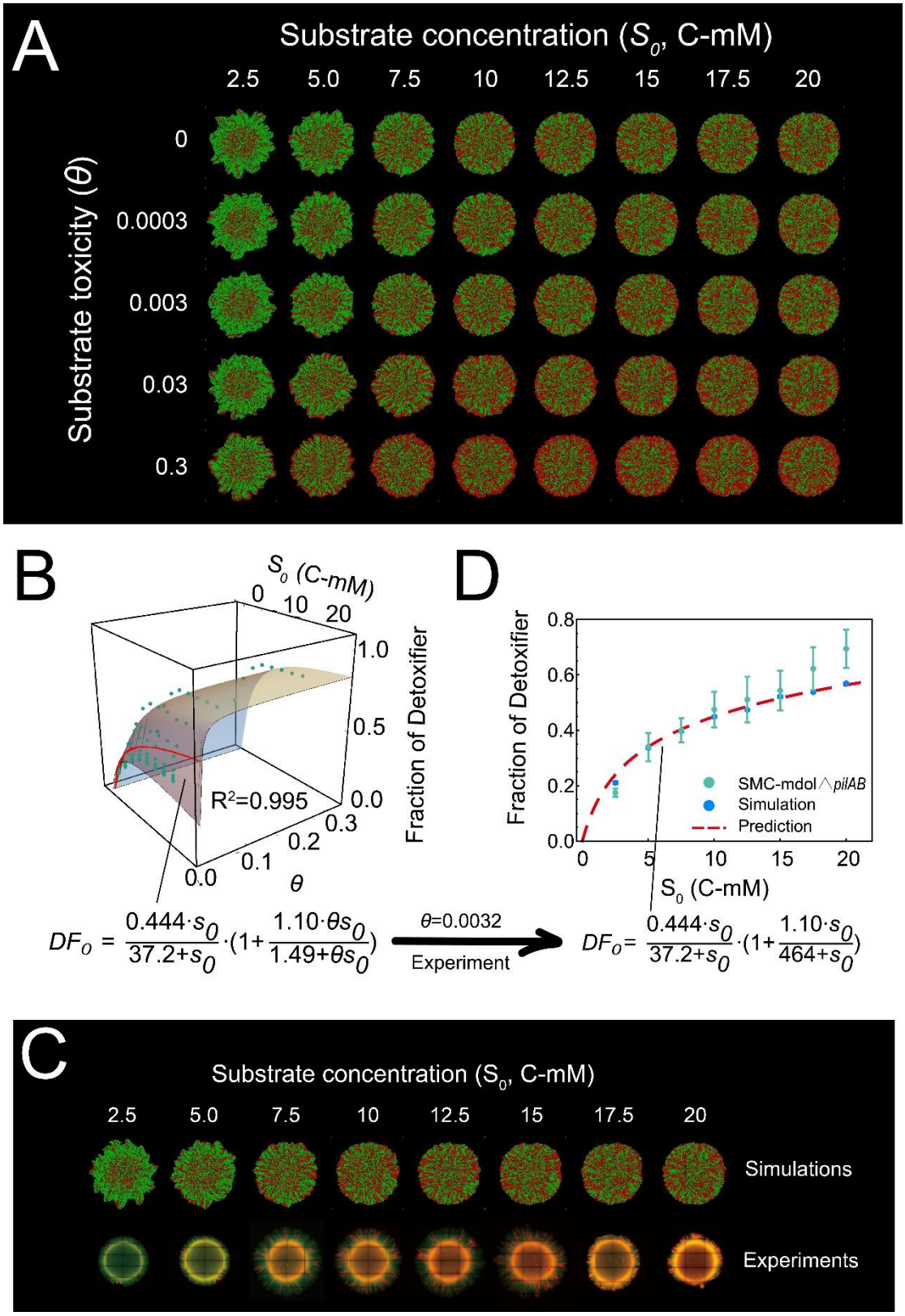

Figure 5 Substrate traits governing the assembly of a microbial community engaged in metabolic division of labor (MDOL) in a spatially structured environment. (A) Representative colony patterns from Individual-based (IB) modelling initialized with

1022 different substrate traits. Detoxifier cells are shown in red, while Embezzler cells are
1023 shown in green. (B) Analysis of community composition in the expanding region of the
1024 colonies from IB simulations across eight kinds of initial substrate concentrations and
1025 five different toxic strength. Plot shows how both substrate concentration and its
1026 toxicity collectively affect the stead-state proportion of Detoxifier. The green dots
1027 denote the simulated stead-state fraction of Detoxifier. The surface shows the plot of
1028 the best fitting function using Eqn. [2]. The Red line in the surface denotes the scenarios
1029 θ=0.0032, which is the toxic strength of salicylate obtained from experimental
1030 measurements. (C) Representative colony patterns from the pattern formation assays of
1031 SMC-mdol△*pilAB*, as well as the IB simulations using the parameters matched with
1032 our synthetic system (Supplementary Table 7), across eight different initial substrate
1033 concentrations. (D) The experimental measured steady-state fractions of Detoxifier in
1034 the expanding region of these colonies is consistent with those from mathematical
1035 predictions. Note that in the plots, substrate concentrations are shown in dimensional
1036 form (S_0, Cmmol/L), but in the predictive functions, the fitting analyses were performed
1037 using its dimensionless form (s_0).
1038

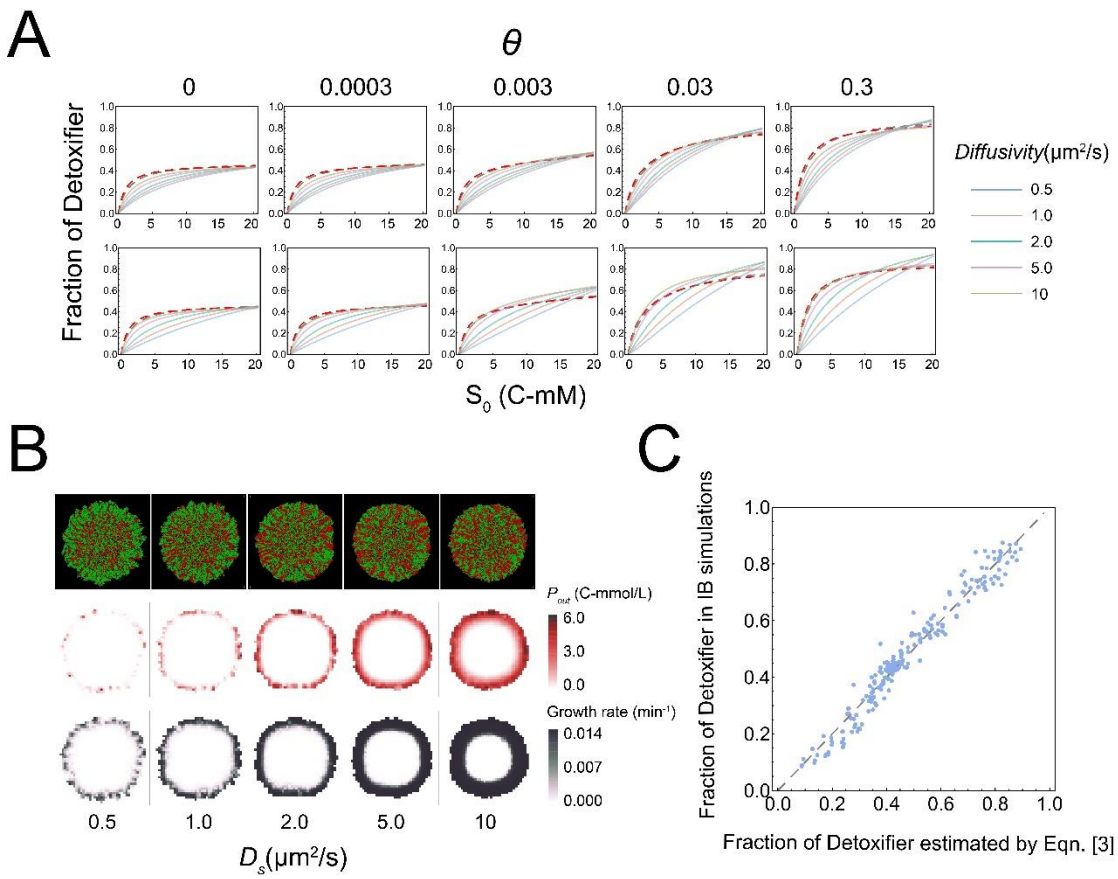

Figure 6 The effects of the diffusion level of substrate, intermediate and product on the assembly of MDOL community. (A) The relationship between initial substrate concentration (S_0) with the steady-state proportion of Detoxifier cells in the expanding region of the colonies, across different substance diffusion level (denoted by different curve colors) and different strength of substrate toxicity (θ, denoted by five subgraphs). First row: diffusion levels of S, I and P (that is D_i, D_i, and D_p) were set to be identical and simultaneously modulated in the simulations. Second row: Diffusion levels of I and P (D_i and D_p) were set as default values shown in Supplementary Table 7, while diffusion levels of S were solely modulated. Other parameters in these simulations were initialized with the default values shown in Supplementary Table 7. The simulation data were then fitted to Eqn. [2] to obtain the curves shown in the plot. The Adjust R^2 values

1051 for these fitting analyses range from 0.994 to 0.997. (B) Diffusion levels of substrate
1052 affected the thickness of cell 'active layer'. Representative colony images (first row),
1053 the corresponding distributions of final product (second row), as well as the
1054 distributions of cell growth rates (third row) in the 2D plane at steady-state, obtained
1055 from individual-based simulations initialized with different diffusion level of substrate.
1056 Shown are the results in which S_0 was set to 10 C-mol/L and θ was 0 (not include
1057 substrate toxicity). In the colony images, Detoxifier cells are shown in red, while
1058 Embezzler cells are shown in green. Thickness of cell 'active layer' is reflected by
1059 thickness of the cell layer that possessing positive growth rate (third row). (C) The
1060 linear correlation between the steady-state frequencies of Detoxifier predicted by Eqn.
1061 [4] and those frequencies obtained by our Individual-based simulations. The dashed
1062 line shows the linear curve in which the predicting results is completely identical to
1063 simulated results. The best fitting value of ks, Fd_{max}, kt, TS_{max}, kd_1, and kd_2 in this case
1064 are 30.8, 0.446, 1.46, 1.05, 14000, and 44.8 respectively.